Available online at www.sciencedirect.com
ScienceDirect
Journal of Catalysis 256 (2008) 126–136
JOURNAL OF CATALYSIS
www.elsevier.com/locate/jcat

Hydrocarbon reactions on MoS_2 revisited, I: Activation of MoS_2 and interaction with hydrogen studied by transient kinetic experiments

Mykola Polyakov [a], Maurits W.E. van den Berg [a], Thomas Hanft [a], Martha Poisot [b], Wolfgang Bensch [b], Martin Muhler [a], Wolfgang Grünert [a,*]

[a] *Laboratory of Industrial Chemistry, Ruhr University Bochum, D-44780 Bochum, Germany*
[b] *Institute of Inorganic Chemistry, Christian Albrechts University Kiel, Kiel, Germany*

Received 3 February 2008; revised 10 March 2008; accepted 10 March 2008

Available online 14 April 2008

Abstract

MoS_2 was prepared by thermal decomposition of ammonium tetrathiomolybdate in inert gas at 723–773 K and activated by procedures involving evacuation at 723 K and/or reduction at different temperatures, predominately 573 K. Bulk and surface properties of these samples were studied by X-ray diffraction (XRD), extended X-ray absorption fine structure (EXAFS), X-ray photoelectron spectroscopy (XPS), nitrogen physisorption, oxygen chemisorption (273 K, pulse mode), and isotope exchange with D_2 to determine the quantity of exchangeable hydrogen. In addition, the quantity of hydrogenation-active surface hydrogen was determined by hydrogenation of ethylene in absence of gas-phase hydrogen. No obvious relationship was found between the S/Mo stoichiometry and the degree of Mo exposure; depending on the pretreatment, exposed Mo ions can be detected by oxygen chemisorption at widely varying quantities while the S/Mo ratio remains $\geqslant 2$. At more severe reduction treatments to remove additional sulfur, the oxygen chemisorption capacity decreases, likely due to migration of defects into the bulk. The reactivity of MoS_2, as expressed by the temperatures required to expose Mo ions and the quantity of exchangeable hydrogen, varies significantly between batches prepared by similar routes. Therefore, thorough surface characterization by a set of techniques including reactivity studies is an indispensable prerequisite for any meaningful study investigating the relationship between catalytic properties with preparation procedures. After activation, MoS_2 holds hydrogen, which is able to hydrogenate ethylene in absence of gas-phase H_2; the quantity of this hydrogenation-active surface hydrogen is not correlated with the hydrogenation activity, however.

Keywords: Molybdenum sulfide; Active sites; Chemisorption; Hydrogen activation; XPS; XAFS

1. Introduction

MoS_2 has been a subject of continuous attention, being a key component of hydrorefining catalysts, and its structural and catalytic properties have been studied in some detail. In particular, the pathways of hydrogen activation have been studied experimentally ([1] and references cited therein, [2–6]) and theoretically [7–13]. Along with its hydrodesulfurization activity, MoS_2 is known to catalyze various hydrocarbon reactions as hydrogenation, *cis–trans* isomerization, double-bond migration, and H/D exchange, as well as the H_2/D_2 scrambling reaction. These reactions were thoroughly investigated by Tanaka and his group, most of whose work has been summarized in Ref. [14].

The work of Tanaka and coworkers suggests that some reactions are specific to particular surface sites. This has been supported by a consistent interpretation of various experiments, particularly studies with labeled hydrocarbons. But some recent theoretical studies have produced findings that contradict most of the reaction mechanisms proposed by Tanaka and coworkers as well as others (cf. [5]). The existence of hydrogen bonded to Mo sites (Mo–H), which is a general ingredient in the reaction mechanisms discussed, has been rejected by most DFT-based studies [8–12]; likewise, a previously reported energy gain of 0.05 eV/H_2 [13] for the formation of Mo–H + –SH from the interaction of H_2 with a sulfur vacancy [13] does not indicate

* Corresponding author. Fax: +49 234 321 4115.
E-mail address: w.gruenert@techem.rub.de (W. Grünert).

0021-9517/$ – see front matter
doi:10.1016/j.jcat.2008.03.007

a stable situation. Some of the disagreement may arise from differences in the surfaces considered. In Ref. [15], the formation of Mo–H species was suggested to occur most likely on triply unsaturated Mo sites, whereas the theoretical studies to date have dealt mostly with saturated surfaces or low degrees of unsaturation.

The methods used to study the interaction of hydrogen with supported or unsupported MoS_2 surfaces have ranged from volumetric or gravimetric adsorption measurements (e.g., [16]) through analysis of exchangeable surface hydrogen by exchange with deuterium (performed mostly through isotope dilution analysis [16]) and TPD [16,17] to vibrational spectroscopy, such as IR [2–4,18,19] or inelastic neutron scattering (INS) [6,20,21]. In the spectroscopic studies, the existence of –SH groups has been well established, whereas evidence for Mo–H species is scarce. At high pressures and temperatures, a second form of adsorbed hydrogen has been detected by INS [6,21], but its assignment remains a matter of debate, absorption of hydrogen molecules [6] and adsorption on basal-plane sulfur anions (after activation on edge planes) [7] having been suggested. Jalowiecki et al. [22] have proposed an interesting alternative technique, close to the catalytic process, that involves the reaction of adsorbed hydrogen with an olefin (isoprene) in a hydrogen-free atmosphere. The method should differentiate adsorbed species available for hydrogenation from spectator species, and the authors assumed that it is possible to count hydrogen on Mo–H sites through the number of hydrogenated molecules [15].

The present work is focused on well-studied simple hydrocarbon reactions, with the intention of using them to probe the surface properties of unsupported MoS_2 prepared through different methods and of other chalkogenide phases. Because such an investigation can produce meaningful results only when performed with well-characterized samples, we used XRD, EXAFS, and various adsorption techniques to elucidate the relationship between the reduction process used to activate the catalyst and the surface properties achieved (i.e., BET surface area, degree of coordinative unsaturation, hydrogen adsorption capability). The literature is full of discrepancies with respect to this relationship, a prominent example being the existence of a maximum degree of coordinative unsaturation for increasing activation severity as reported by Kalthod and Weller [23] versus the claim of monotonously increasing Mo exposure at decreasing S/Mo atomic ratio derived by Jalowiecki et al. [15] from work with MoS_2 of (nominally) similar preparation. Consequently, in Part I of this work we report the findings of structural and surface studies conducted on several batches of MoS_2 prepared by thermolysis of ammonium thiomolybdate. The data show that this MoS_2 preparation is very sensitive to subtle changes in process conditions, giving materials with strongly differing properties.

Although our findings emphasize the importance of thorough structural and surface characterization and the need for a more detailed study of this preparation route, they also allow us to draw some general conclusions regarding, for example, the lack of correlation between S/Mo stoichiometry and coordinative unsaturation of the surface, the decrease in the latter under severe reduction conditions, and the amount of surface hydrogen capable of hydrogenating ethylene in the absence of gas-phase H_2. In Part II of this work [24], we describe the influence of reductive activation on the activity in test reactions (i.e., ethylene hydrogenation, butene-2 *cis–trans* isomerization, H_2/D_2 scrambling). Our findings suggest that these reactions can be used to probe coordinatively unsaturated Mo sites (Mo_{cus}) with different numbers of sulfur vacancies.

2. Experimental

2.1. Materials

MoS_2 was prepared by thermal decomposition of ammonium tetrathiomolybdate [$(NH_4)_2MoS_4$, ATTM] in flowing inert gas. The ATTM, which had been initially treated in a ball mill at 1000 rpm for 1 h, was inserted in a rotating furnace preheated to 473 K. With nitrogen flowing over the sample, the temperature was increased to 773 K at a rate of 2.5 K min^{-1}, then maintained at 773 K for 10 min. Data from three identically prepared batches [$MoS_2(A_1)$, $MoS_2(A_2)$, and $MoS_2(A_3)$] are reported here, to allow evaluation of the reproducibility of the synthesis. A fourth batch [$MoS_2(B)$] was prepared by a slightly different procedure—a two-stage process, involving heating the ball-milled precursor at 553 K in Ar for 45 min in a first step, followed by intermediate milling for 30 min, and finally thermolysis in Ar at 723 K for 75 min (tubular furnace). A total of 10 g of $MoS_2(A_1)$ was made, whereas the remaining batches were available only in limited amounts. For reference purposes, a microcrystalline MoS_2 [MoS_2(cryst)] was obtained through a similar route but with very slow temperature ramps and a final thermolysis at 1273 K for 60 h (total duration of synthesis, 7 days). All samples were handled and stored in Ar after preparation. The basic properties of the batches are summarized in Table 1.

2.2. Physicochemical characterization

Chemical elemental analyses were performed with a EURO Vector EA combustion analyzer using zinc sample holders filled with 2–3 mg of sample. The samples were heated up to 1000 °C under oxygen atmosphere, and the gases were detected by a thermoconductivity cell. Powder XRD patterns were recorded with a STOE STADI-P instrument using monochromatized Cu$K_{\alpha 1}$ radiation ($\lambda = 1.54056$ Å).

EXAFS spectra at the MoK edge (20,000 eV) were measured in transmission mode at X1 station of Hasylab (Desy, Hamburg, Germany), using a Si(311) monochromator detuned to 50% of maximum intensity to exclude higher harmonics in the X-ray beam. The spectrum of a Mo foil was measured simultaneously for calibration purposes. Samples were pressed into discs of suitable thickness in a glove box. The discs were sealed airtight in Kapton tape before the measurements, which were made at liquid-nitrogen temperature. Data treatment was carried out using the software package VIPER for Windows [25]. A Victoreen polynomial was fitted to the pre-edge region for background subtraction. The smooth atomic

Table 1
Bulk stoichiometry, BET surface area, and primary particle size of MoS_2 samples used in this study

	$MoS_2(A_1)$	$MoS_2(A_2)$	$MoS_2(A_3)$	$MoS_2(B)$	MoS_2(cryst)
Preparation[a]	773 K, 10 min rotary	773 K, 10 min rotary	773 K, 10 min rotary	723 K, tubular 75 min	1270 K, tubular 60 h
S/Mo	2.40	2.41	2.31	2.24	2.01
BET surface area[b], $m^2\,g^{-1}$	20.8	29.1	15	12.0	0.3[c]
Particle size[d], nm	11.0	13.0	7.8	10.4	27.8

[a] Ex ATTM, see text for details; temperature time and reactor type of second decomposition step are given.
[b] After evacuation at 473 K.
[c] Krypton physisorption.
[d] From XRD, using Scherrer equation with (002) reflection.

background, μ_0, was estimated using a smoothing cubic spline. Fourier analysis of the k^3-weighted experimental function $\chi = (\mu - \mu_0)/\mu_0$ was performed with a Kaiser window. For the determination of structural parameters, theoretical references calculated by the FEFF8.10 code [26] were used.

X-ray photoelectron spectra were recorded with a Scienta/Specs/Prevac Surface analysis system equipped with a monochromatized Al anode and a Scienta SES 2002 electron analyzer. To avoid contact with air, samples (particularly after activation) were transferred from the glove box to the load lock of the instrument by means of a sample transfer shuttle (Prevac, with in-house modifications). The potential of this shuttle can be illustrated by a test run, in which a reduced sample of an MnO_x/SiO_2 oxygen scavenger [27] was transferred from the glove box to the spectrometer and back with no change in its light-green color. With the samples in place, the Mo 3d, S 2p, O 1s, N 1s, and C 1s lines were measured (X-ray source at 55 mA and 14 kV). The data were processed with CasaXPS Version 2.2.82 software. The binding-energy (BE) scale was referenced to the Mo 3d signal of the sulfide state (Mo $3d_{5/2} = 229.1$ eV), because adventitious carbon could not be detected on the activated samples. Where both lines were available [in, e.g., the initial $MoS_2(A_2)$], the C 1s line was at 284.4 eV with this calibration.

N_2 physisorption isotherms were measured with a Quantachrome Autosorb-1 MP instrument to establish BET surface areas and pore size distributions. Before these measurements, the samples were evacuated at different temperatures. Pore size distributions were derived from the desorption branches using the BJH formalism.

2.3. Catalysis and related measurements

Although the results of catalytic measurements are reported in Part II of this paper, here we briefly describe the main features of the catalytic setup used to obtain the results reported in this part (see Part II for more details [24]). A catalytic micro fixed-bed reactor is at the heart of the setup in which the flow scheme can be switched between closed-cycle (batch) and continuous-flow mode through a four-way valve. The reactor is contained in a smaller loop (ca. 20% of the reaction cycle volume), which can be separated from the gas lines by switching another four-way valve; thus, the reactor can be detached from the setup and inserted into a glove box. This allows the reactor to be loaded with air-sensitive catalysts or activated catalyst to be transferred to the glove box for investigation by other techniques (e.g., XAFS, XPS). The gas line section containing the reactor (loop) also can be switched between the reaction cycle and a vacuum system by operating a six-way valve (at which it is installed instead of a sampling loop). This minimizes the risk of surface contamination between activation in vacuum and subsequent procedures.

In the present study, MoS_2 (usually 0.1 g per run) was typically investigated after three different activation treatments: (a) evacuation (rotary pump) at 723 K for 4 h (designated $\mathbf{V}_{723}$; previously used by Tanaka et al. [14]), (b) evacuation with subsequent reduction in H_2 (10% in He) at 573 K for 3 h (designated $\mathbf{V}_{723}/\mathbf{R}_{573}$), and (c) reduction in H_2 (10% in He) at 573 K for 3 h *without* previous thermoevacuation (designated $\mathbf{R}_{573}$). In some cases, the reduction temperature differed from 573 K; this is reflected in the designation. Occasionally, the sequence of the treatments was changed in the combined activation (i.e., $\mathbf{R}_{573}/\mathbf{V}_{723}$ instead of $\mathbf{V}_{723}/\mathbf{R}_{573}$). After the activation steps, one of the following procedures was performed:

- *Oxygen chemisorption* (*OCS*). OCS was measured in the pulse mode using the catalytic setup in flow mode. After activation, the catalyst was cooled to 273 K in He. Pulses of 0.304 μmol O_2 were dosed into the He carrier gas, and the effluent was monitored by (calibrated) mass spectrometry (Pfeiffer QME 125). The reproducibility of the OCS measurements was tested by repeating a complete experiment with $MoS_2(A_3)$ (i.e., weighing, $\mathbf{R}_{573}$ activation, chemisorption) five times, which yielded an average OCS of 33.8 $\mu mol\,g^{-1}$, with a mean square deviation of 1.1 $\mu mol\,g^{-1}$.
- *Hydrogen chemisorption* (*HCS*). HCS was measured by the same technique as OCS. The catalyst was activated by $\mathbf{V}_{723}$, the pulse size was 5.35 μmol H_2, and the measurement temperatures were 298, 473, and 573 K.
- *Determination of exchangeable surface hydrogen* (H_{exc}). The amount of surface hydrogen was determined by exchange with D_2 with the setup in the flow mode. After activation, the catalyst was cooled to 473 K in 10% H_2/Ar, at which point the carrier gas was replaced by pure Ar and the temperature was maintained until the $m/e = 2$ QMS signal was constant (ca. 10 min). After further cooling to room temperature, the reactor was rapidly reheated up to

573 K in a slow flow of D_2 (22 ml/min, 10% D_2 in Ar), and the quantity of HD that evolved was determined by calibrated mass spectrometry. In a special series, the catalyst was cooled in 10% H_2/Ar to other temperatures than 473 K before switching to Ar to check for weakly adsorbed hydrogen. Such a temperature is referred to as a *minimum adsorption temperature* [T_{ads}(min)]. The reproducibility of the H_{exc} measurements was tested by repeating a complete experiment with $MoS_2(A_3)$ (weighing, $\mathbf{R}_{573}$ activation, determination of H_{exc} at a minimum adsorption temperature of 295 K) four times, which yielded an average H_{exc} of 213 μmol g^{-1}, with a mean square deviation of 14 μmol g^{-1}.

- *Determination of hydrogen active in hydrogenation* (H_{hyd}). For this experiment, 0.8 g of catalyst was activated and subsequently cooled to 298 K, switching from hydrogen to He flow at different temperatures. The reaction cycle (492 ml) was filled with a mixture containing 6.52 mbar of ethylene in He, which was first circulated over the catalyst at room temperature for ca. 20 min. Then the reactor was inserted into the oven to rapidly increase the temperature to 473 K. After ca. 20 min at 473 K, the temperature was further raised to 573 K. The choice of the reaction temperature of 473 K was guided by observations that at temperatures below 440 K, significant deactivation by deposition of hydrocarbon material occurred even in the presence of hydrogen [24]. Product analysis was performed by calibrated mass spectrometry. The experiment was carried out with different activation treatments ($\mathbf{R}_{573}$, $\mathbf{V}_{723}/\mathbf{R}_{573}$, and $\mathbf{R}_{573}/\mathbf{V}_{723}$); for more details, see [28].

3. Results

3.1. Initial samples

Table 1 summarizes the stoichiometry and the BET surface areas of the MoS_2 materials used in this study. The samples prepared by decomposition of ATTM at ca. 720–770 K contained excess sulfur and had widely varying initial BET surface areas. The high-temperature MoS_2(cryst) was stoichiometric and had a very low BET surface area.

Powder XRD patterns of MoS_2 samples are shown in Fig. 1. Whereas MoS_2(cryst) displays narrow diffraction lines, the reflections of the MoS_2 batches with excess sulfur are broad, as reported in earlier studies with similar preparations [29,30]. The particle size along the *c* axis [from the (002) diffraction peak at $2\Theta = 14°$] was estimated using Scherrer's equation (cf. Table 1); the values were between 8 and 13 nm for the samples with excess sulfur (corresponding to 15–20 layers), but almost 30 nm for the high-temperature preparation. The peaks characteristic of the lengths (diameters) of the MoS_2 slabs [(101) and (100) at $2\Theta \approx 33°$] are superimposed and thus are not suitable for determining the correlation lengths. The shape of the reflections suggests that they are of the same order of magnitude, however.

EXAFS spectra of the same samples are displayed in Fig. 2 (modulus of the Fourier-transformed k^3-weighted spectra). In

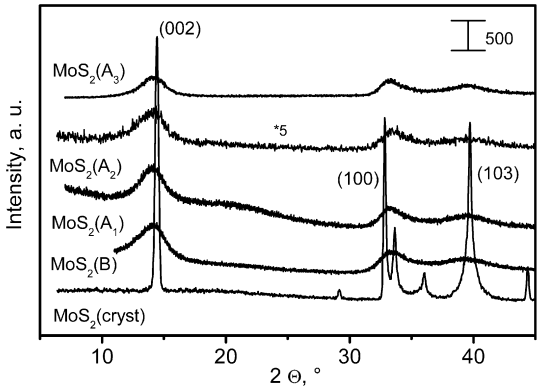

Fig. 1. X-ray diffractograms of MoS_2 prepared via different routes.

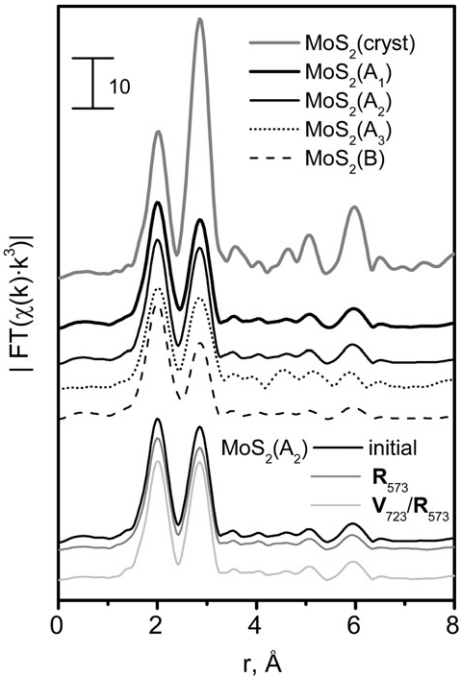

Fig. 2. EXAFS spectra of MoS_2 prepared via different routes and of a MoS_2 batch ($MoS_2(A_2)$) after different activation treatments.

the spectrum of MoS_2(cryst), two major scattering events due to the next S and Mo neighbors [2.02 and 2.83 Å, respectively (all distances uncorrected)] can be seen, along with peaks at ca. 5.1 and 6.05 Å due to other Mo neighbors (enhanced by multiple scattering [30]). The latter are almost completely missing in the spectra of the sulfur-rich MoS_2 samples, in which a significant amplitude decay is visible for the first Mo–Mo shell. Model fits were made with FEFF parameters adjusted to reproduce the spectrum of MoS_2(cryst) with parameters close to the crystallographic ones (Table 2, first entry). These fits yielded Mo–Mo coordination numbers (CNs) between 4.4 and 3.1 for the remaining samples (Table 2). By correlation with the diameter of the MoS_2 slabs suggested previously [31], the Mo–Mo CN of 3.6 found for $MoS_2(A_1)$ transforms to a slab size of ca. 2.7 nm. This estimate relies on the assumption that in these samples, the distortion of the Mo–Mo distances at the surface relative to the bulk is similar to those used in previous studies [30,31], which can be justified given the similar preparation conditions.

Table 2
Parameters of structural models obtained from the spectra summarized in Fig. 2

Sample	Shell	r, Å	C.N.	$10^3\sigma^2$, Å^{-2}	ΔE, eV
MoS_2(cryst)	S	2.408 ± 0.003	5.2 ± 0.2	3.3 ± 0.3	7.5 ± 0.5
	Mo	3.160 ± 0.002	6.6 ± 0.2	2.4 ± 0.1	4.1 ± 0.4
$MoS_2(A_1)$	S	2.411 ± 0.002	5.3 ± 0.2	4.2 ± 0.3	6.9 ± 0.4
	Mo	3.157 ± 0.002	3.6 ± 0.2	3.2 ± 0.2	4.5 ± 0.6
$MoS_2(A_2)$	S	2.408 ± 0.002	4.7 ± 0.2	3.7 ± 0.3	6.6 ± 0.4
	Mo	3.153 ± 0.003	4.0 ± 0.2	3.4 ± 0.2	2.5 ± 0.6
$MoS_2(A_2)$, after $\mathbf{R}_{573}$	S	2.409 ± 0.002	4.8 ± 0.1	4.0 ± 0.2	7.6 ± 0.3
	Mo	3.157 ± 0.002	4.2 ± 0.2	4.1 ± 0.2	4.7 ± 0.5
$MoS_2(A_2)$, after $\mathbf{V}_{723}/\mathbf{R}_{573}$	S	2.409 ± 0.002	5.0 ± 0.2	3.9 ± 0.3	7.6 ± 0.4
	Mo	3.155 ± 0.002	4.3 ± 0.2	3.7 ± 0.2	4.4 ± 0.5
$MoS_2(A_3)$	S	2.403 ± 0.003	4.5 ± 0.2	2.9 ± 0.5	7.0 ± 0.4
	Mo	3.169 ± 0.005	4.4 ± 0.3	4.0 ± 0.5	6.2 ± 0.8
MoS_2(B)	S	2.417 ± 0.002	5.3 ± 0.2	4.7 ± 0.3	7.0 ± 0.3
	Mo	3.160 ± 0.003	3.1 ± 0.2	4.4 ± 0.3	5.6 ± 0.7

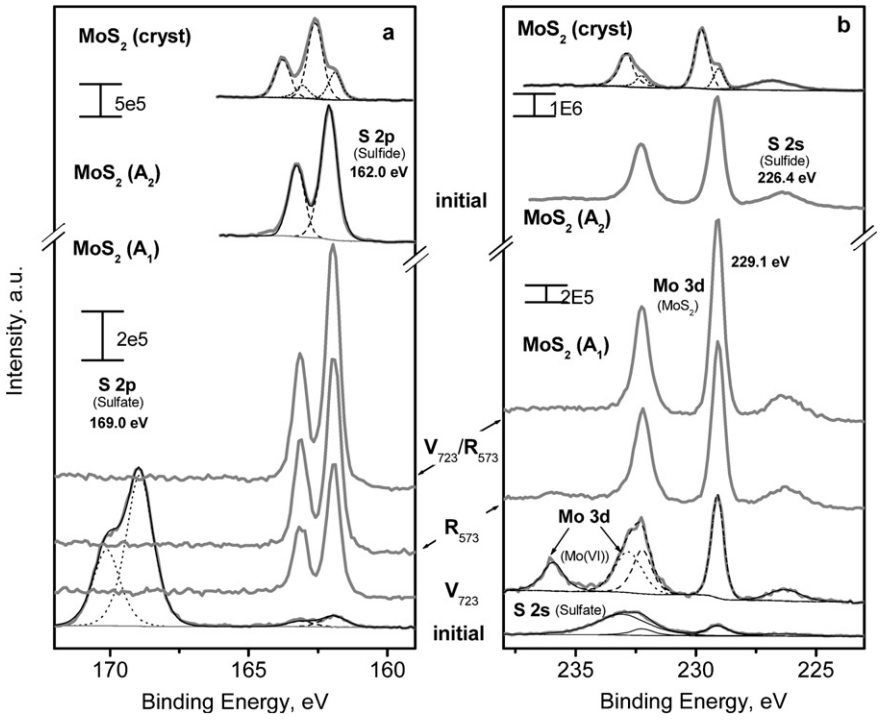

Fig. 3. XP spectra of MoS_2 prepared via different routes and of $MoS_2(A_1)$ after different activations. (a) S 2p region; (b) Mo 3d region.

The estimated slab sizes of the remaining sulfur-rich samples are between 5 and 2 nm. To investigate a possible influence of sintering processes during the activation, EXAFS spectra of $MoS_2(A_2)$ also were measured after typical activation treatments (Fig. 2; Table 2). The slight increase in the Mo–S and Mo–Mo CN seen in these data are within the limits of experimental accuracy.

Fig. 3 shows XPS spectra of MoS_2 samples in the as-prepared state. The spectra of MoS_2(cryst) and $MoS_2(A_2)$ reveal that the surface of these samples is clean, with no lines except those characteristic of S in sulfide (Fig. 3a) and Mo(IV) in MoS_2 (Fig. 3b). The spectra of $MoS_2(A_3)$ are not shown, because they are very similar to those of $MoS_2(A_2)$. In MoS_2(cryst), all major lines are paralleled by satellites, which may arise from a differential charging effect. The reason for this feature is not clear, but it obviously is not due to an impurity species. Very small oxygen signals (not shown) are thought to arise from structural defects. In MoS_2(B) (spectra not shown), a weak signal due to elemental sulfur can be seen, along with the signals typical of MoS_2.

The surface of the as-received $MoS_2(A_1)$ sample turned out to be heavily contaminated, although there was no indication for this in the elemental analysis. In the surface of $MoS_2(A_1)$, the sulfur was present largely as sulfate (Fig. 3a). The Mo 3d line was hardly visible (Fig. 3b), whereas an intense N 1s line was observed (not shown). From the line intensities, the N/S(sulfate) atomic ratio was estimated to be ca. 1; that is, the surface was covered by ammonium (hydrogen)

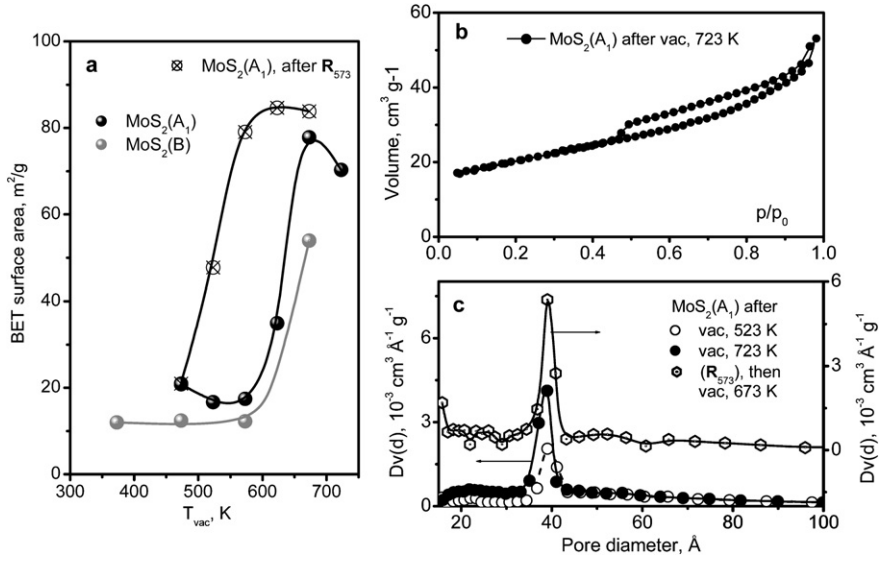

Fig. 4. Porosity analysis of MoS_2 by nitrogen physisorption. (a) Development of BET surface area with temperature of thermoevacuation for two batches; comparison with sample previously treated in hydrogen ($\mathbf{R}_{573}$). (b) Adsorption isotherm (example). (c) Pore-size distributions (BJH, desorption branch) of MoS_2 after different treatments. The vacuum treatments indicated differ from the standard vacuum activations (e.g., $\mathbf{V}_{723}$) in their duration (2 h instead of 4 h).

Table 3
Oxygen chemisorption (OCS) capacity, concentration of exchangeable hydrogen (H_{exc}), and S/Mo ratios after different activation procedures

Treatment	$MoS_2(A_1)$			$MoS_2(A_2)$	$MoS_2(A_3)$	$MoS_2(B)$
	S/Mo	OCS capacity, μmol O_2/g	H_{exc}, μmol HD/g (H/Mo)	OCS capacity, μmol O_2/g	OCS capacity, μmol O_2/g	OCS capacity, μmol O_2/g
Initial	2.40	0	Imp.[a]	0	–	–
$\mathbf{V}_{723}$	2.11	6.5[c]	1 (0.0004)	11	1	5
$\mathbf{V}_{723}/\mathbf{R}_{473}$[b]	n. d.	11[c]	131 (0.043)	23	–	–
$\mathbf{V}_{723}/\mathbf{R}_{573}$	2.04	28	115 (0.038)	30	22	33
$\mathbf{R}_{473}$[b]	n. d.	12[c]	121 (0.040)	62	16	–
$\mathbf{R}_{573}$	2.10_5	60	109 (0.036)	35 (44[d])	34	–
$\mathbf{R}_{573}/\mathbf{V}_{723}$	2.00	29	–	–	–	–

[a] Impossible, HD exchange does not proceed over initial sample.
[b] As $\mathbf{V}_{723}/\mathbf{R}_{573}$ (or $\mathbf{R}_{573}$), but with reduction temperature 473 K.
[c] Probably affected by surface impurity, see text.
[d] After only 1 h reduction at 573 K, MoS_2(cryst) did not adsorb oxygen after any of the activation treatments and, hence, gave no results in the HD exchange either.

sulfate species. For this reason, the surface also was studied after different activations. Evacuation at 723 K ($\mathbf{V}_{723}$) completely decomposed the sulfate and ammonium species, but along with the lines characteristic of MoS_2, a Mo(VI) signal, apparently arising from Mo oxide species in the surface region, remained (Fig. 3b). The observation that thermoevacuation of contaminated MoS_2 cleans the surface of everything but residual Mo(VI) oxide species has been reported on the basis of IR evidence [19]. Fig. 3 shows also that reduction in hydrogen at 573 K with or even without previous thermoevacuation ($\mathbf{V}_{723}/\mathbf{R}_{573}$ or $\mathbf{R}_{573}$) is suited for cleaning the surface effectively.

3.2. Activation and surface properties

Fig. 4 characterizes the effect of thermal activation on BET surface area. The BET surface area of the as-prepared sulfur-rich materials was found to increase strongly during evacuation at elevated temperatures, even though the materials previously had been exposed to such temperatures for a short time during the synthesis. This increase is obviously related to a loss of excess sulfur, as confirmed by elemental analysis (Table 3). Indeed, elemental sulfur was found on cold surfaces of the setup after the experiment. In the adsorption isotherms (see the example shown in Fig. 4b), capillary effects were seen only in the desorption branch (IUPAC classification type H3), which indicates slit pores. In the pore-size distributions, a rather narrow peak at ca. 4 nm grew strongly at higher activation temperatures (Fig. 4c). The increased BET surface area on thermoevacuation was observed for all samples [$MoS_2(A_2)$, 66.3 m^2/g after $\mathbf{V}_{723}$; $MoS_2(A_3)$, 73.4 m^2/g after $\mathbf{V}_{723}$], indicating that it was not induced by the surface contaminations initially present in $MoS_2(A_1)$.

With $MoS_2(A_1)$, the temperature dependence of the BET surface area also was studied after initial reduction of the catalyst at 573 K without previous thermoevacuation ($\mathbf{R}_{573}$). This

activation left the BET surface area near the initial value of 21 $m^2\ g^{-1}$ (cf. Fig. 4a), but when the material was subsequently evacuated at elevated temperatures, the increase in BET surface area occurred at a much lower temperature.

Table 3 summarizes the oxygen chemisorption capacities measured with the four MoS_2 batches after different activation treatments. The table also reports quantities of exchangeable hydrogen (H_{exc}) for $MoS_2(A_1)$ and compares these values with the S/Mo stoichiometries achieved. The latter demonstrate that the activation treatments used here were not suitable for creating significant sulfur deficiencies; as confirmed by repeated runs for all of the activations studied, S/Mo stoichiometries of 2.05–2.10 (identical in the limits of experimental error) were found for $\mathbf{V}_{723}$, $\mathbf{R}_{573}$, and $\mathbf{V}_{723}/\mathbf{R}_{573}$, although the BET surface areas developed differed dramatically (e.g., between $\mathbf{V}_{723}$ and $\mathbf{R}_{573}$; cf. Fig. 4). Only thermoevacuation subsequent to reduction ($\mathbf{R}_{573}/\mathbf{V}_{723}$) resulted in a further slight decrease in the S/Mo ratio, but definitely not to a sulfur deficiency.

As known from earlier studies [14], thermoevacuation ($\mathbf{V}_{723}$) creates coordinatively unsaturated Mo sites (Mo_{cus}), but the oxygen chemisorption capacity is low. The values of the different batches scatter between 1 and 11 μmol/g. An effect on vacancy formation of the surface Mo oxide species remaining on $MoS_2(A_1)$ after $\mathbf{V}_{723}$ (Fig. 3) cannot be discerned at this stage, because a much lower OCS capacity (1 μmol g^{-1}) was found with one of the clean materials [$MoS_2(A_3)$]. Reduction at 573 K ($\mathbf{R}_{573}$) increased the OCS capacity significantly, but the values differed significantly between some of the batches (Table 3), and, in the case of $MoS_2(A_2)$, even a dependence on treatment duration was noted. The scatter between the results obtained with different MoS_2 batches was smaller when the reduction was preceded by an evacuation at 723 K. In most cases, the OCS capacity was around 30 μmol O_2/g after this $\mathbf{V}_{723}/\mathbf{R}_{573}$ treatment, but with a smaller value for $MoS_2(A_3)$. Remarkably, the same OCS capacity also was found when the surface of $MoS_2(A_1)$ activated by $\mathbf{R}_{573}$ (resulting in 60 μmol g^{-1}) was subsequently subjected to $\mathbf{V}_{723}$ (cf. Table 3); however, the reactivity of these surface states differed greatly despite the identical OCS capacity, as we discuss in more detail in Part II.

To elucidate the origin of the discrepancies in the data of Table 3, the influence of reduction temperature (without previous thermoevacuation) on the OCS capacities was studied; the results are summarized in Fig. 5. Apparently, the effect of reduction differed greatly among the batches, but a peak OCS capacity was a common feature. Above the peak temperature, the total exposure of surface Mo ions again decreased, although in our experiments, H_2S was clearly present in the effluent at the higher reduction temperatures as well. This peak temperature was 470 K (or below) for $MoS_2(A_2)$, ca. 570 K for $MoS_2(A_1)$, and 670 K for $MoS_2(A_3)$. The peak OCS capacities ranged from 44 to 62 μmol g^{-1}. The high OCS capacity measured with $MoS_2(A_2)$ after $\mathbf{R}_{473}$ (62 μmol g^{-1}) was indirectly confirmed by a run in which a higher reduction temperature of 573 K was applied to this material for only 1 h; the resulting value of 44 μmol g^{-1} is significantly greater than that found after a 3-h reduction (35 μmol g^{-1}; cf. Table 3). With

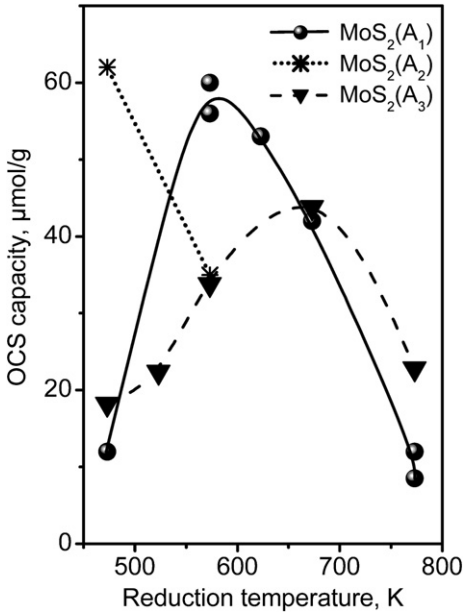

Fig. 5. Dependence of the oxygen chemisorption capacity of $MoS_2(A)$ after reduction at different temperatures (compare also Table 3).

previous thermoevacuation at 723 K, the material exhibited no exceptional behavior. The OCS capacity created by $\mathbf{V}_{723}/\mathbf{R}_{573}$ exceeded that found after $\mathbf{V}_{723}/\mathbf{R}_{473}$.

The amount of exchangeable hydrogen (H_{exc}) was measured after all of the activations with $MoS_2(A_1)$ (Table 3) but only for some of the activations with the other samples. As expected, the concentration of exchangeable hydrogen was much larger after the MoS_2 surface had been in contact with H_2. Whereas the value found after $\mathbf{V}_{723}$ was near the detection limit, the hydrogen-treated surfaces produced 110–130 μmol HD/g, indicating no pronounced differences among the treatments as was seen with oxygen chemisorption. It should be noted that in several cases (e.g., after activations at 473 K), the quantities of exchanged hydrogen exceeded the OCS capacity dramatically. This was even more pronounced with $MoS_2(A_2)$, which yielded completely different H_{exc} data. After $\mathbf{R}_{573}$, a H_{exc} quantity of 590 μmol g^{-1} was found (H/Mo = 0.19; compare this with the OCS capacity of 35 μmol g^{-1} (Table 3). After $\mathbf{R}_{473}$, H_{exc} was 340 μmol g^{-1} (H/Mo = 0.11; OCS, 62 μmol g^{-1}; Table 3). Again, we can see significant differences in the surface reactivity of batches prepared following the same protocol.

TPD studies in the literature [17] suggest that MoS_2 accommodates a considerable quantity of weakly bound hydrogen. We checked this for $MoS_2(A_1)$ after $\mathbf{R}_{573}$ by varying the minimum adsorption temperature, T_{ads}(min) (see Section 2), before interacting the catalyst with D_2. The results, shown in Fig. 6, demonstrate a steady increase of H_{exc} with decreasing minimum adsorption temperature, suggesting a considerable variation in binding strengths between hydrogen and the surface. A temperature of 500 K seems appropriate to differentiate strongly and weekly bound hydrogen; beyond 500 K, the amount of exchangeable hydrogen no longer decreased. The highest quantity of exchangeable hydrogen measured (on cooling to room temperature) corresponded to a H/Mo ratio of 0.07, with 1/3 of this of the stable form.

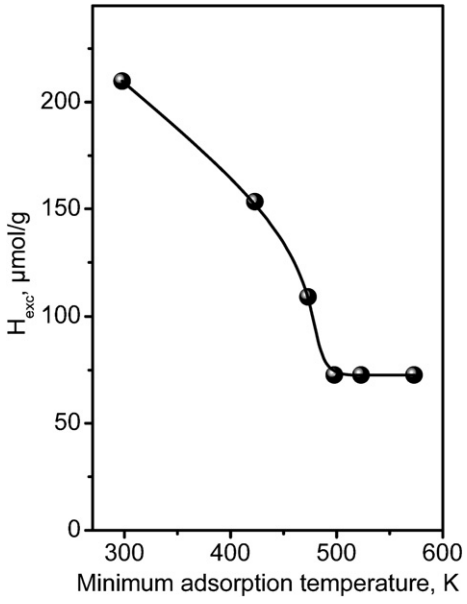

Fig. 6. Dependence of the quantity of exchangeable hydrogen on MoS_2 (activated by $\mathbf{R}_{573}$) on the lowest temperature in contact with H_2 (during a cooling stage from the adsorption temperature of 573 K).

Dynamic hydrogen chemisorption was performed with $MoS_2(A_1)$ after $\mathbf{V}_{723}$ to investigate whether the stable hydrogen form was created in a rapid process (e.g., by reaction with Mo_{cus}). No dynamic hydrogen consumption was found at room temperature and at 473 K. It should be noted that despite the rather large pulse size used in these measurements, chemisorption onto the coordinatively unsaturated sites indicated by OCS (i.e., two times 7 µmol/g) would have been clearly detected by mass spectrometry. At 573 K, the consumption was 62 µmol/g. We did not attempt to differentiate which part of this hydrogen was adsorbed or consumed for the creation of new vacancies by H_2S formation.

Fig. 7 summarizes the observations made during hydrogenation of ethylene with surface hydrogen using the simple reductive activation $\mathbf{R}_{573}$. The experiment was conducted with three different minimum adsorption temperatures to explore possible interference by weakly adsorbed hydrogen, which could possibly desorb into the gas phase and obscure the results. As shown in Fig. 7a, a surface cooled in hydrogen to room temperature desorbed large quantities of H_2 on heating to 473 K and even more on a further temperature increase to 573 K. The total ethane formation in this experiment (including the stage at 573 K) was 67.5 µmol/g. It is obvious that most of this ethane was formed from gas-phase hydrogen, which may have originated from any type of H species initially present on the surface; however, closer inspection of Fig. 7a shows that after the reactor was placed in the oven to heat it up to 473 K, hydrogen desorption lagged behind ethane formation by ca. 1 min, possibly indicating some hydrogenation by adsorbed species.

The runs with higher minimum adsorption temperatures confirm this observation. Here hydrogen desorption was much less intense, although clearly still present. As shown in Fig. 7b ($T_{ads}(\text{min}) = 473$ K), the delay of hydrogen desorption behind ethane formation was ca. 6 min. The ethane trace increased linearly, certainly influenced by the gas-phase hydrogen formed. As shown in Fig. 7c ($T_{ads}(\text{min}) = 573$ K), the delay of hydrogen desorption relative to ethane formation was less pronounced, because the former was very weak; however, the rate of ethane formation was the highest just after heating to 473 K and almost leveled off after ≈10 min. It exhibited the behavior expected for the reaction of a limited amount of species, whereas the $m/e = 2$ trace demonstrated only a very small, almost linear increase. This indicates that hydrogenation occurred predominately with surface hydrogen in this case. Ascribing the ongoing increase in the $m/e = 30$ trace to hydrogenation by gas-phase hydrogen, the dashed line in Fig. 7c can be used to estimate the concentration of hydrogenation-active surface hydrogen; the result is $H_{hyd} = 1.7$ µmol H_2/g. Apparently, the degree of ethane formation does not depend on the minimum adsorption temperature in the 473–573 K range; the amount of hydrogenation-active hydrogen that can be derived from the $m/e = 30$ trace in Fig. 7b ($T_{ads}(\text{min}) = 473$ K) is of the same order of magnitude. Fig. 7a indicates that more loosely bound hydrogenation-active hydrogen may have been present, because

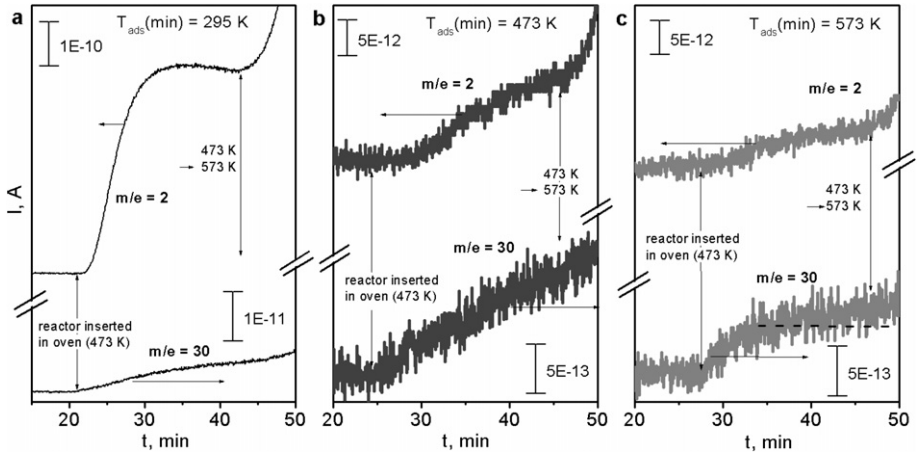

Fig. 7. Hydrogenation of ethylene with surface hydrogen of MoS_2 (activation – $\mathbf{R}_{573}$). Runs with different minimum adsorption temperature: (a) $T_{ads}(\text{min}) = 295$ K; (b) $T_{ads}(\text{min}) = 473$ K; (c) $T_{ads}(\text{min}) = 573$ K. Signals intensities for $m/e = 2$ (H_2) and 30 (ethane) plotted vs real time for a reaction temperature of 473 K, including the rapid heating stage (see label "reactor inserted in oven") and further heating to 573 K (label "473 K → 573 K").

the ethane released before hydrogen desorption resulted in an estimated H_{hyd} concentration of ≈7 μmol H_2/g.

The same experiment also was performed after activations including thermoevacuation ($\mathbf{V}_{723}/\mathbf{R}_{573}$, $\mathbf{R}_{573}/\mathbf{V}_{723}$, in the latter case after a 60-min readsorption of hydrogen at 573 K). The amount of H_{hyd} obtained with $T_{ads}(\text{min}) = 573$ K was 0.8 μmol H_2/g after $\mathbf{V}_{723}/\mathbf{R}_{573}$ and 2.5–3.5 μmol H_2/g after $\mathbf{R}_{573}/\mathbf{V}_{723}$, with no difference in the limits of experimental error for $T_{ads}(\text{min}) = 473$ K. These data are certainly subject to considerable uncertainty due to the very small effects and should be considered upper limits, because the contribution due to gas-phase hydrogen cannot be clearly differentiated from that of surface hydrogen. Nonetheless, the evolution of ethane in a time segment in which almost no hydrogen desorption occurred clearly shows that active hydrogen was available on the surface, at a quantity an order of magnitude lower than the degree of coordinative unsaturation.

4. Discussion

Previous research has provided no conclusive description of either the hydrogen species on MoS_2 and their role in hydrocarbon reactions or the active sites required for these reactions. Although the presence of surface –SH groups has been well established, the ability of the Mo_{cus} ions to adsorb hydrogen remains a matter of debate, the existence and role of absorbed hydrogen is unclear, and a possible role of short-lived activated hydrogen species (on Mo_{cus}) has not been discussed in much detail. Analogously, it is generally accepted that such reactions as olefin hydrogenation, *cis–trans* isomerization, and H_2/D_2 scrambling proceed on coordinatively unsaturated Mo sites, but the differentiation of these sites (and evaluation of true turnover numbers) is hampered by the lack of differentiation in standard adsorption studies. Volumetric measurements provide only cumulative data. IR investigations do differentiate sites with different Mo exposure, but extinction coefficients for the adsorbed probe molecules are difficult to establish. Perhaps for this reason, Jalowiecki et al. correlated their catalytic activities with the degree of Mo exposure using site abundances derived from S/Mo stoichiometries through model calculations [15] without relying on (oxygen) chemisorption data. With the present study, we believe to contribute relevant observations to advance the discussion and inspire new approaches to solving these problems.

Although the preparation of our MoS_2 catalysts differed somewhat from that used in many other studies (i.e., thermal decomposition of ATTM in inert gas instead of H_2S/H_2), our materials have similar properties as reported in the literature, as characterized by such techniques as XRD, elemental analysis, and XAFS. The MoS_2 samples consisted of platelets 2–5 nm in diameter stacked 8–13 nm high containing a considerable amount of excess sulfur. The BET surface areas measured with the as-prepared samples were within the range reported in the literature (although much larger BET surface areas—up to 115 $m^2\,g^{-1}$—also have been reported [32]). This excess sulfur was removed by the thermal activation treatments. Jalowiecki et al. [15] reported S/Mo stoichiometries (from full elemental analysis) of 2.0–1.7 after 12 h reduction in hydrogen above 600 K; thus, the S/Mo stoichiometries of 2.0–2.1 after our milder activation treatments (4 h evacuation at 723 K and/or 3 h reduction at 573 K) were as expected. In Ref. [23], S/Mo ratios >2 were found even after reduction at 773 K, in clear conflict with the findings of Jalowiecki et al. [15]. Whether this contradiction is due to the simplified methodology used in our work (i.e., thermogravimetry during reoxidation to MoO_3) or to a real difference in sample properties remains unclear.

The BET surface areas of our (sulfur-rich) MoS_2 batches were all between 10 and 30 $m^2\,g^{-1}$ but grew significantly during thermal activation, reaching 55–70 $m^2\,g^{-1}$ after $\mathbf{V}_{723}$. A more detailed study of $MoS_2(A_1)$ revealed a narrow peak in pore size distribution at around 4 nm, which was superimposed over a broad mesopore distribution and developed strongly on thermoevacuation. Similar nitrogen adsorption/desorption isotherms have been reported previously [30], but only for a material prepared through a different route (i.e., MoO_3–KSCN solid-state reaction). According to the shape of the hysteresis, the peak at 4 nm arose from slit pores, which apparently were initially filled with elemental sulfur. The behavior of the BET surface area of $MoS_2(A_1)$ after activation by reduction ($\mathbf{R}_{573}$) (Fig. 4a) was rather unexpected. Although the S/Mo stoichiometry was the same as after $\mathbf{V}_{723}$ (Table 3), the BET surface area was not increased (ca. 20 $m^2\,g^{-1}$, compared with ≈70 $m^2\,g^{-1}$ after $\mathbf{V}_{723}$). During subsequent thermoevacuation, it grew at much lower temperatures than in the unreduced sample and without pronounced changes in the S/Mo ratio. The latter observation may suggest that after $\mathbf{R}_{573}$, the pores were free but not accessible, with the increased BET surface area on thermoevacuation due to opening, rather than emptying, of pores.

In our study, we used oxygen chemisorption to evaluate the degree of coordinative Mo unsaturation, even though sites of different Mo exposure (^{1}M, ^{2}M, ^{3}M sites) cannot be differentiated by this technique. In the past, oxygen chemisorption was studied mostly by volumetric or gravimetric techniques at 195 K. At room temperature, static techniques were found to produce large values, suggesting the presence of side reactions, whereas the dynamic technique produced 67% of the volumetric result at 195 K [33]. In a similar comparison [i.e., transferring a MoS_2(B) sample after $\mathbf{V}_{723}/\mathbf{R}_{523}$ to the Autosorb 1-MP via the glove box], we found 44 μmol g^{-1} by volumetry at 195 K, compared with 33 μmol g^{-1} by the dynamic technique at 273 K (cf. Table 3). Consequently, we conclude that our data closely reflect the degree of coordinative unsaturation of the surface, possibly underestimating it by 20–25%.

Our data demonstrate that oxygen chemisorption may occur on samples with S/Mo ratios >2, as reported in Ref. [23] where, however a simplified elemental analysis technique was used. Apparently, there is no relationship between the degree of Mo exposure and the S/Mo ratio; at S/Mo = 2.11, OCS capacities of 7 and 60 μmol g^{-1} were found, depending on the sample history (Table 3). On reduction of $MoS_2(A_1)$ at temperatures >573 K (Fig. 5), H_2S was clearly detected in the effluent, but the degree of Mo exposure decreased significantly, to a greater extent than was reported earlier by Kalthod and Weller [23]. These apparent contradictions may stem from the presence of resid-

ual elemental sulfur after our mild activation treatments, which would outbalance the small stoichiometric deficit of the MoS_2 surface. The loss of OCS capacity with increasing reduction temperature (above the peak temperatures, which are different for different batches; Fig. 5) may be due to increasing particle size (due to sintering), incorporation of excess sulfur into the surface, or diffusion of surface defects into the bulk. Our XAFS data (Fig. 2; Table 2) do not indicate pronounced changes in the platelet dimensions on thermal treatment at 723 K, and the decrease in BET surface area begins only above 673 K (Fig. 3); therefore, we prefer the latter explanation, at least for temperatures <700 K.

Striking differences in the effect of activation treatment on the degree of Mo exposure were found on the surfaces of MoS_2 batches created by the same person through the same route. These differences would have been hardly apparent on conventional physicochemical characterization involving XRD, elemental analysis, BET (even with varied pretreatment temperature), and XAFS. Apparently, the preparation route is critically influenced by parameters that were not well controlled in our preparations. Thus, the considerable scatter of experimental OCS data, as reported in the literature (see, e.g., [23,33–35]), does not come as a surprise. The ammonium (hydrogen) sulfate impurities initially present on the surface of one of our samples cannot explain these discrepancies, which were found in samples with clean surfaces as well (cf. Fig. 5). We believe that the discrepancies among our batches arise largely from differences in microstructure that affect defect creation and mobility. The somewhat larger Mo–Mo EXAFS CNs for the more stable $MoS_2(A_3)$ may indicate a somewhat higher degree of ordering in this sample, however, the fits depend on many parameters, and the effect is hardly beyond the limits of experimental accuracy. Thus, more work is required to substantiate this hypothesis.

The amount of hydrogen on the MoS_2 surface that can be exchanged with D_2 had no correlation with the degree of Mo exposure characterized by oxygen chemisorption (Table 3). From $MoS_2(A_1)$, 110–130 μmol HD/g was released after $\mathbf{R}_{573}$ and $\mathbf{R}_{473}$, even though the OCS capacity changed by a factor of 5. On $MoS_2(A_2)$, 590 μmol HD/g was found at an OCS capacity of just 35 μmol g^{-1}. Although the presence of Mo–H cannot be ruled out based on this observation, most of the hydrogen must have been be in the form of –SH groups or absorbed hydrogen. But this was unlikely under our conditions, because absorbed hydrogen was observed only after treatment at elevated H_2 pressure [20]. Even though the measured OCS capacities did not exactly match the number of exposed Mo atoms (*vide supra*), in several cases the quantity of exchangeable H greatly exceeded the number of sulfide ions adjacent to the vacancies present, particularly when the sample was cooled in hydrogen to room temperature (Fig. 6). Therefore, spillover appears to be involved in adsorption and desorption, as was reported earlier for MoS_2-containing systems [36]. This is also supported by the observation that in the H/D exchange experiments, a 1-h inert gas purge at 473 K (573 K) decreased the exchangeable amount by 50% (67%), even though the QMS signal apparently was constant after 5–10 min. Obviously, very slow desorption, possibly involving a transport step, was occurring.

The experiment depicted in Fig. 7 confirms that hydrogen-treated MoS_2 was able to hydrogenate an olefin in absence of gas-phase hydrogen, as described previously [15]. To avoid results obscured by weakly bound hydrogen desorbing into the gas phase, thorough desorption of the latter is mandatory. This is obvious from the results obtained after cooling the activated sample in hydrogen to room temperature; under these conditions, the hydrogen found in the ethane product exceeded the OCS capacity, whereas the gas-phase H_2 concentration (also fed by the surface hydrogen initially present) remained far from zero. Thus, the hydrogen traced in this run clearly involved contributions from SH groups.

When the rate of H_2 desorption was kept low, the presence of hydrogenation-active surface hydrogen (H_{hyd}) could be clearly demonstrated (Fig. 7, right panels). The quantity determined in the present study (<2 μmol g^{-1}) was almost an order of magnitude lower than the values of 10–40 μmol g^{-1}reported previously [15]. This hydrogen was strongly held because it survived (short) desorption at temperatures above 473 K (during cooling in inert gas from 573 K). It represents only a small part of the hydrogen held on the surface under these conditions (ca. 75 μmol g^{-1}; cf. Fig. 6). According to the results of previous studies [14], this hydrogen should be adsorbed on Mo_{cus} sites. In Part II, we show that the hydrogenation activity of MoS_2 differed by two orders of magnitude after $\mathbf{R}_{573}$ and $\mathbf{R}_{573}/\mathbf{V}_{723}$, which gave very similar H_{hyd} quantities, demonstrating a lack of correlation between activity and the quantity of H_{hyd} as measured by our method. However, we did find results suggesting that the amount of hydrogenation-active hydrogen increased when weakly bound hydrogen was included (Fig. 7a). The method used here was too coarse to permit a reliable determination of its quantity, but a more detailed investigation of this species may be promising.

The problem of hydrogen involved in the hydrogenation reaction is discussed in more detail in Part II.

5. Conclusion

MoS_2 prepared by thermal decomposition of ammonium tetrathiomolybdate in inert gas at 723–773 K exposed Mo ions (detected by oxygen chemisorption) after mild activation procedures that maintained an S/Mo ratio of $\geqslant 2$. No obvious relationship between the S/Mo stoichiometry and the degree of Mo exposure was found. When the MoS_2 was activated in hydrogen, the degree of Mo exposure reached a maximum at intermediate reduction temperatures; this did not occur when the sample had been thermoevacuated before reduction. The reactivity of MoS_2 (i.e., temperature required to expose Mo, quantity of exchangeable hydrogen) may change significantly between samples prepared similarly; therefore, a thorough surface characterization, including chemisorption studies, is essential to any meaningful catalytic study. Along with –SH groups, MoS_2 holds hydrogen, which is able to hydrogenate ethylene in absence of gas-phase H_2. This hydrogen can survive short ex-

posure to inert gas at 573 K, but its quantity is not correlated with the degree of hydrogenation activity.

Acknowledgments

Financial support was provided by the German Science Foundation (Grants Gr 1447/15 and Be-1653/11). The authors thank D. Silber for assisting with the experiments shown in Fig. 7 and Susanne Buse for providing the physisorption measurements.

References

[1] J. Polz, H. Zeilinger, B. Müller, H. Knözinger, J. Catal. 120 (1989) 22.
[2] P. Ratnasamy, J.J. Fripiat, Trans. Faraday Soc. 66 (1970) 2897.
[3] N.-Y. Topsoe, H. Topsoe, J. Catal. 139 (1993) 641.
[4] H. Payen, S. Kasztelan, J. Grimblot, J. Mol. Struct. 174 (1988) 71.
[5] M. Breysse, E. Furimsky, S. Kasztelan, M. Lacriox, G. Perot, Catal. Rev.-Sci. Eng. 44 (2002) 651.
[6] P.N. Jones, E. Knözinger, W. Langel, R.B. Moyes, J. Tomkinson, Surf. Sci. 207 (1989) 159.
[7] A.B. Anderson, Z.Y. Al-Saigh, W.K. Hall, J. Phys. Chem. 92 (1988) 803.
[8] L.S. Byskov, M. Bollinger, J.K. Norskov, B.S. Clausen, H. Topsoe, J. Mol. Catal. A 163 (2000) 117.
[9] L.S. Byskov, J.K. Norskov, B.S. Clausen, H. Topsoe, J. Catal. 187 (1999) 109.
[10] S. Cristol, J.F. Paul, E. Payen, D. Bougeard, S. Clemendot, F. Hutschka, J. Phys. Chem. B 106 (2002) 5659.
[11] S. Cristol, J.F. Paul, E. Payen, D. Bougeard, S. Clemendot, F. Hutschka, J. Phys. Chem. B 104 (2002) 11220.
[12] V. Alexiev, R. Prins, T. Weber, Phys. Chem. Chem. Phys. 3 (2001) 5326.
[13] M. Sun, A.E. Nelson, J. Adjaye, Catal. Today 105 (2005) 36.
[14] K.-I. Tanaka, T. Okuhara, Catal. Rev.-Sci. Eng. 15 (1977) 249.
[15] L. Jalowiecki, A. Aboulaz, S. Kasztelan, J. Grimblot, J.P. Bonelle, J. Catal. 120 (1989) 108.
[16] T. Komatsu, W.K. Hall, J. Phys. Chem. 95 (1991) 9966.
[17] X.S. Li, Q. Xin, X.X. Gou, P. Grange, B. Delmon, J. Catal. 137 (1992) 385.
[18] A.A. Tsyganenko, F. Can, A. Travert, F. Maugé, Appl. Catal. A 268 (2004) 189.
[19] F. Maugé, J. Lamotte, N.S. Nestorenko, O. Manoilova, A.A. Tsyganenko, Catal. Today 70 (2001) 271.
[20] C. Sampson, J.M. Thomas, S. Vasudevan, C.J. Wright, Bull. Soc. Chim. Belg. 90 (1981) 1215.
[21] P. Sundberg, R.B. Moyes, J. Tomkinson, Bull. Soc. Chim. Belg. 100 (1991) 967.
[22] L. Jalowiecki, M. Daage, J.P. Bonelle, A. Tchen, Appl. Catal. 16 (1985) 1.
[23] D.G. Kalthod, S. Weller, J. Catal. 95 (1985) 455.
[24] M. Polyakov, M. Poisot, W. Bensch, M. Muhler, W. Grünert, J. Catal. 256 (2008) 137 (this issue).
[25] K.V. Klementiev, VIPER for Windows (Visual Processing in EXAFS Researches), freeware, http://www.desy.de/~klmn/viper.html.
[26] A.L. Ankudinov, B. Ravel, J.J. Rehr, S.D. Conradson, Phys. Rev. B 58 (1998) 7565.
[27] C.R. McIlwrick, C.S.G. Phillips, J. Phys. E 6 (1973) 1208.
[28] M. Polyakov, Ph.D. thesis, Bochum, 2007.
[29] Y. Iwata, K. Sato, T. Yoneda, Y. Miki, Y. Sugimoto, A. Nishijima, H. Shimada, Catal. Today 34 (1998) 353.
[30] C. Calais, N. Matsubayashi, C. Geantet, Y. Yoshimura, H. Shimada, A. Nishijima, M. Lacroix, M. Breysse, J. Catal. 174 (1998) 130.
[31] T. Shido, R. Prins, J. Phys. Chem. B 102 (1998) 8426.
[32] P. Hou, H. Wise, J. Catal. 89 (1982) 469.
[33] T.A. Bodrero, C. Bartholomew, J. Catal. 84 (1983) 145.
[34] S.J. Tauster, T.A. Pecoraro, R.R. Cianelli, J. Catal. 63 (1980) 515.
[35] D.G. Kalthod, S. Weller, J. Catal. 98 (1986) 572.
[36] L. Jalowiecki, J. Grimblot, J.P. Bonelle, J. Catal. 126 (1990) 101.